crystals

MDPI

Article

Coordination Flexibility of Zn(II) in Trimesate-Based Metal–Organic Frameworks: Formation of Distinct Secondary Building Units

Giovanni Bella, Francesco Nicolò, Giuseppe Bruno, Amine Assel and Antonio Santoro *

Department of Chemical, Biological, Pharmaceutical and Environmental Sciences, University of Messina, Viale F. Stagno d'Alcontres 31, 98166 Messina, Italy; gbella@unime.it (G.B.); fnicolo@unime.it (F.N.); gbruno@unime.it (G.B.); assel.amine@gmail.com (A.A.)
* Correspondence: antonio.santoro@unime.it; Tel.: +39-0906765762

Abstract

Two zinc(II)-trimesate metal–organic frameworks were synthesized under hydrothermal conditions and structurally characterized by single-crystal X-ray diffraction. Although both compounds originate from the same Zn(II)-benzene-1,3,5-tricarboxylate (BTC) chemical system, they crystallize in different space groups and exhibit distinct coordination environments and secondary building units (SBUs). One framework adopts a cubic structure and is built from a binuclear Zn paddlewheel type SBU, characterized by a short Zn–Zn internuclear distance and four μ_2-bridging carboxylate groups. In contrast, the second framework crystallizes in a tetragonal lattice and features mixed Zn(II) coordination environments, with the coexistence of tetrahedral and octahedral metal centers assembled into a fundamentally different SBU. The comparison between these two structures highlights the coordination flexibility of Zn(II) and the sensitivity of Zn–BTC frameworks to crystallization conditions, such as solvent composition. These results underline the importance of detailed crystallographic analysis in revealing SBU diversity and provide insight into how variations in local coordination chemistry can lead to distinct framework architectures from identical chemical building blocks.

Keywords: Zn(II) MOF; crystallographic analysis; paddlewheel SBU; benzene-1,3,5-tricarboxylate (BTC) MOF; single crystal X-ray diffraction; crystal engineering

1. Introduction

Nanomaterials and their derivatives exhibit unique photonic, electronic, magnetic and chiroptical properties that arise from their structural characteristics in the nanoscale domain [1–10]. In this broad landscape, metal–organic frameworks (MOFs) represent a prominent class of crystalline coordination polymers composed of metal ions or metal clusters interconnected by multitopic organic ligands into extended networks. Owing to their modular nature, MOFs exhibit exceptional structural diversity, allowing structural tunability in terms of topology, pore size, and functionality through suitable selection of metal nodes, organic linkers and, importantly, synthetic conditions [11–17]. Within the framework of reticular chemistry, which describes the design of extended crystalline networks through the assembly of pre-defined molecular building units, MOFs can be viewed as assemblies of well-defined units whose geometry and connectivity are reflected in pore dimensions, architectural features and tunable physicochemical properties [11–18]. Zinc(II)

Check for updates

Academic Editor: Laurent Plasseraud

Received: 30 March 2026
Revised: 20 April 2026
Accepted: 23 April 2026
Published: 28 April 2026

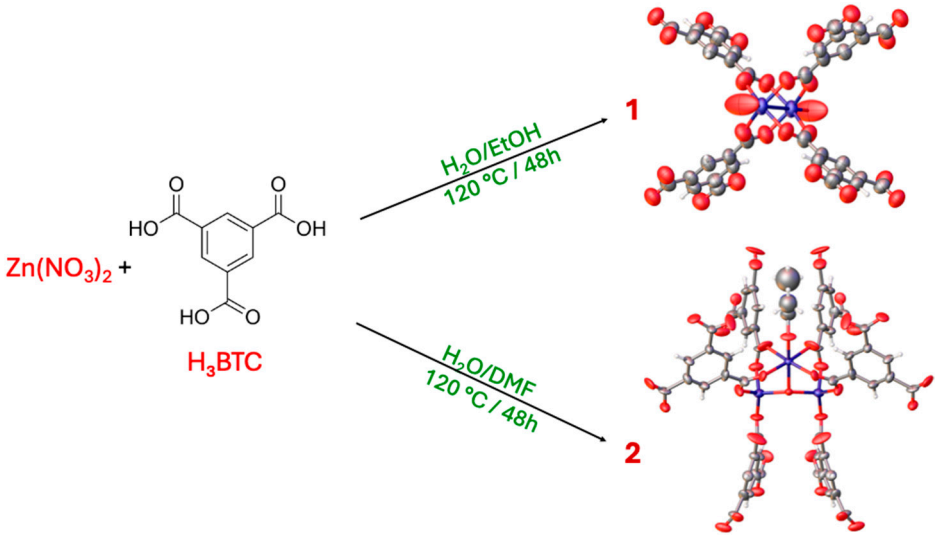
Copyright: © 2026 by the authors. Licensee MDPI, Basel, Switzerland. This article is an open access article distributed under the terms and conditions of the Creative Commons Attribution (CC BY) license.

is one of the most extensively employed metal atoms in MOF synthesis due to its closed-shell electronic configuration, flexible coordination behavior, chemical stability, and an ionic radius compatible with a wide range of carboxylate-based ligands [19–25]. Zn(II) centers can adopt different coordination geometries such as tetrahedral, trigonal bipyramidal, or octahedral, that can be chosen varying the synthetic conditions, the nature of the partner ligands and the stoichiometry. The flexible coordination behavior of Zn(II) often leads to the formation of distinct SBUs, defined as recurring inorganic or metal–organic clusters that act as nodes within the framework [26–28]. SBUs encode the local coordination chemistry of the metal centers and play a fundamental role in determining framework dimensionality, topology, and structural stability [29–31]. Importantly, SBUs are not uniquely dictated by the chemical identity of the building blocks, but may vary depending on crystallization conditions, including the presence of auxiliary ligands, solvent molecules of different nature, or guests that stabilize specific coordination environments [32–36]. Among polycarboxylate ligands, benzene-1,3,5-tricarboxylic acid (trimesic acid, H_3BTC) has attracted particular interest due to its trigonal geometry and ability to bridge multiple metal centers simultaneously. Upon full deprotonation, BTC3- can coordinate through a variety of binding modes, including monodentate, chelating, and bridging carboxylate groups, often leading to the formation of multinuclear SBUs in Zn–based systems [37–39]. Numerous Zn–BTC frameworks have been reported, displaying significant structural diversity in terms of metal coordination environments, cluster nuclearity, and overall network topology [21,38–47]. Solvent molecules may act as templating agents, participate directly in metal coordination, or occupy framework voids, thereby stabilizing specific SBUs and influencing the final network architecture [46–50]. As a result, minor changes in crystallization conditions can yield distinct frameworks or solvated forms that are not preliminarily identifiable from stoichiometry alone. In this context, single-crystal X-ray diffraction (SCXRD) is essential for resolving the coordination environments, ligand binding modes, and SBU organization of Zn–BTC frameworks [51–53]. In this work, we report the synthesis and SCXRD structural characterization of two Zn(II)-trimesate frameworks obtained under different crystallization conditions. Although both structures originate from the same Zn–BTC system and the same stoichiometry, they exhibit distinct SBUs. Despite the extensive literature on Zn–BTC frameworks, the relationship between modest changes in crystallization conditions and SBU selection remains not fully predictable, particularly when identical metal-ligand systems are employed. In many cases, small changes in solvent composition or reaction environment can lead to markedly different coordination modes and framework topologies, highlighting the need for detailed comparative crystallographic studies. One framework (**1**) features a binuclear Zn unit characterized by a short Zn–Zn separation, four μ_2-bridging carboxylate groups in the equatorial plane, and an axially coordinated solvent molecule, consistent with a paddlewheel type $Zn_2(O_2CR)_4$ motif. In contrast, the second framework (**2**) displays non-equivalent Zn(II) coordination environments, involving tetra- and hexa-coordinated metal centers interconnected by BTC ligands and stabilized by coordinated solvent molecules, resulting in a radically different SBU and network architecture. By comparing these two structures, this study highlights how the coordination flexibility of Zn(II) combined with crystallization conditions governs SBU selection in Zn–BTC frameworks, leading to alternative framework architectures derived from identical chemical building blocks.

2. Materials and Methods

The single crystal of **1** reactor and heated at 120 °C for 48 h. After completion of the reaction, the system was obtained by hydrothermal synthesis using zinc nitrate and benzene-1,3,5-tricarboxylic acid (H_3BTC). Equimolar aqueous solutions (5×10^{-3} M) of

$Zn(NO_3)_2$ and H_3BTC were mixed in a 1:1 (v/v) water/ethanol solvent system. The resulting mixture was sealed in a batch was allowed to cool slowly to room temperature over 24 h. Colorless single crystals were obtained, among which a crystal of suitable size and quality was selected for SCXRD analysis. The single crystal of **2** was prepared under hydrothermal conditions starting from zinc nitrate and H_3BTC. Equimolar solutions (5×10^{-3} M) of $Zn(NO_3)_2$ and H_3BTC were combined in a 1:1 (v/v) water/Dimethylformamide (DMF) solvent mixture. The reaction was conducted in batch mode at 120 °C for 48 h, followed by slow cooling to room temperature over 24 h. The two synthesis are summarized in the Scheme 1.



Scheme 1. Reaction scheme for compound **1** and **2**.

The choice of solvent systems was guided by the different coordination behavior of protic and aprotic solvents. While ethanol is expected to act primarily as a weakly coordinating medium, favoring regular carboxylate bridging modes, DMF can directly coordinate to metal centers, potentially stabilizing higher coordination numbers and more complex local environments. These differences were expected to influence the formation of distinct secondary building units during the crystallization process. Colorless single crystals suitable for single-crystal X-ray diffraction were isolated from the resulting solution. Suitable crystals were selected, and their diffraction data were collected at room temperature using a single-crystal Bruker ASX Inch. APEX-II CCD diffractometer, Madison, WI, USA and the APEX2 package (v.2024) [54,55], which was used for data reduction and structure solution (SHELXT (v.2024) [51]), while refinement was carried out using the full-matrix least-squares refinement on F^2 of SHELXL (v.2024) [52] in OLEX2 (v.2024) [56], which also prepared the publication material. The non-hydrogen atoms were refined anisotropically, while the aromatic H atoms were introduced in calculated positions and their bond geometry and isotropic displacement parameters were constrained to ride on their parent atoms. The crystal packings of both compounds are governed by the high symmetry of the 3D framework, with the coordinated solvent molecules (water and DMF, respectively) being highly disordered at the axial positions of the Zn center located on a special crystallographic site. In compound **1**, the hydrogens of the disordered coordinated water were omitted owing to the lack of a reasonable interpretation of their significant electron density residuals surrounding the O atom. In both crystal structure models, the presence of disordered solvent in the cavities of the corresponding porous 3D-network has been treated by the solvent mask method in Olex2 Package [56]. Selected crystallographic parameters and

structural determination features are provided in Table 1. All chemicals were purchased from Merck, Darmstadt, Germany.

Table 1. Comparison of crystallographic and structural features of the two Zn–BTC frameworks.

Feature	1	2
CCDC code	2539925	2539926
Crystal system	Cubic	Tetragonal
Space group	$Fm\bar{3}m$	I4cm
Unit cell parameters (Å)	$a = b = c = 26.582(2)$	$a = b = 20.586(4)$; $c = 17.797(5)$
Unit cell volume (Å^3)	18782(5)	7542(3)
Molecular unit (ASU + solvent)	$C_6H_4O_5Zn$	$C_{21}H_{13}NO_{14}Zn_3$
Z	48	8
Crystal model quality Final R indexes [I $\geq 2\sigma$ (I)]	$R_1 = 0.0382$, $wR_2 = 0.0986$ GooF (F^2) = 0.956	$R_1 = 0.0533$, $wR_2 = 0.1526$ GooF (F^2) = 1.063
Crystallographically independent Zn sites	1	2
Zn coordination environments	Equivalent Zn(II) centers	Non-equivalent Zn(II) centers
Zn coordination number(s)	5 (4 equatorial + 1 axial)	4 (tetrahedral) and 6 (octahedral)
Zn–Zn interaction (Å)	2.968(1)	Not observed
Secondary building unit (SBU)	Binuclear $Zn_2(O_2CR)_4$	Mixed-coordination Zn–based SBU
SBU nuclearity	Binuclear	Polynuclear/extended
Carboxylate coordination mode	μ_2-bridging (equatorial)	Bridging and chelating modes
Axial/terminal ligands	Coordinated solvent (H_2O)	Coordinated solvent (DMF)
Role of solvent	Axial ligand stabilizing Zn_2 SBU	Coordination and stabilization of mixed Zn environments
Framework dimensionality	3D	3D
Overall framework symmetry	High	Lower

3. Results

3.1. Synthesis and Crystallization

Although both frameworks were obtained from the same Zn(II)-BTC chemical system, their crystallization under different solvent compositions resulted in distinct SBUs and coordination environments. In particular, hydrothermal synthesis in a water/ethanol mixture leads to the formation of a binuclear Zn paddlewheel type SBU, characterized by uniform metal coordination environments. In contrast, crystallization of **2** from a water/DMF mixture yields a framework featuring mixed Zn(II) coordination environments, with the coexistence of tetrahedral and octahedral Zn centers. These observations suggest that solvent composition may play a role in modulating Zn(II) coordination preferences during framework assembly. Protic solvents such as water and ethanol may favor more regular carboxylate bridging modes, promoting the formation of binuclear SBUs, whereas the presence of a coordinating polar aprotic solvent such as DMF may stabilize higher coordination numbers and heterogeneous local environments. These findings are consistent with previous observations in MOF chemistry, where solvent molecules can act not only as reaction media but also as structure-directing agents, influencing both the nuclearity and geometry of the resulting SBUs. While no definitive mechanistic conclusions can be drawn from the present data alone, the comparison between these two structures highlights the sensitivity of Zn–BTC frameworks to marginal variations in crystallization conditions

and underscores the importance of solvent environment and thermal parameters in SBU selection. A systematic investigation of the synthetic plan would be required to fully elucidate the mechanisms governing the formation of these distinct architectures.

3.2. Crystal Structure of the Zn–BTC Framework of Compound **1**

Compound **1** crystallizes in the cubic space group $Fm\bar{3}m$ and is characterized by a highly symmetric three-dimensional framework. The asymmetric unit contains one Zn(II) center, which participates in the formation of a binuclear Zn_2 SBU located at the intersection of three orthogonal crystallographic mirror planes. In the crystal packing it can be observed that each Zn(II) ion is coordinated by four oxygen atoms belonging to four distinct carboxylate groups from BTC ligands, arranged in an approximately square-planar equatorial environment, as described in Figure 1. In addition, one oxygen atom from a coordinated solvent molecule occupies an axial position, completing the coordination preference of the metal center. Two such Zn(II) centers are linked through four μ_2-bridging carboxylate groups, giving rise to a $Zn_2(O_2CR)_4$ core. The presence of a short Zn–Zn separation (2.968(1) Å) confirms the binuclear nature of this SBU. This coordination motif is consistent with a paddlewheel-type SBU [19,21]. The BTC ligands act as multitopic linkers, connecting adjacent Zn_2 SBUs and propagating the structure into a three-dimensional network. The high crystallographic symmetry of the framework results in a regular arrangement of these SBUs throughout the lattice, as depicted in Figure 2.

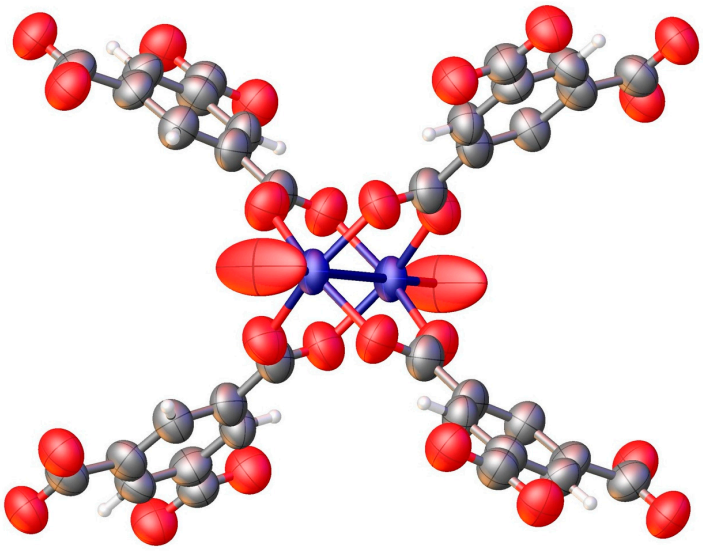


Figure 1. ORTEP representation (50% probability ellipsoids) of the binuclear $Zn_2(O_2CR)_4$ secondary building unit in the cubic Zn–BTC framework of **1**, showing the four μ_2-bridging carboxylate groups in the equatorial plane and the axially coordinated water molecule. Atom labels are omitted for clarity; full labeling is reported in the representation of the asymmetric unit in Figure S1 of Supporting Information.

3.3. Crystal Structure of the Zn–BTC Framework of Compound **2**

Conversely, the MOF **2** crystallizes in the tetragonal space group I4cm and exhibits a markedly different coordination scheme. The asymmetric unit contains two crystallographically independent Zn(II) centers, displaying distinct coordination geometries.

One Zn(II) site adopts a tetrahedral coordination environment defined by three oxygen atoms from BTC carboxylate groups and one μ_3-bridging oxygen atom belonging to the trinuclear Zn–based unit. The second Zn(II) site is hexa-coordinated, with an octahedral geometry defined by oxygen atoms from carboxylate groups and coordinated solvent molecules, as illustrated in Figure 3. No short Zn–Zn separations indicative of direct metal-

metal interactions are observed in this structure, ruling out the presence of a binuclear paddlewheel motif. The coexistence of tetra- and hexa-coordinated Zn(II) centers leads to the formation of a mixed-coordination SBU, fundamentally different from the binuclear unit observed in the cubic framework. BTC ligands bridge these non-equivalent Zn sites through different carboxylate coordination modes, generating an extended three-dimensional architecture stabilized by coordinated solvent molecules. The lower symmetry of the tetragonal lattice reflects the increased complexity of the local coordination environments and the reduced regularity of the SBUs (see Figure 4).

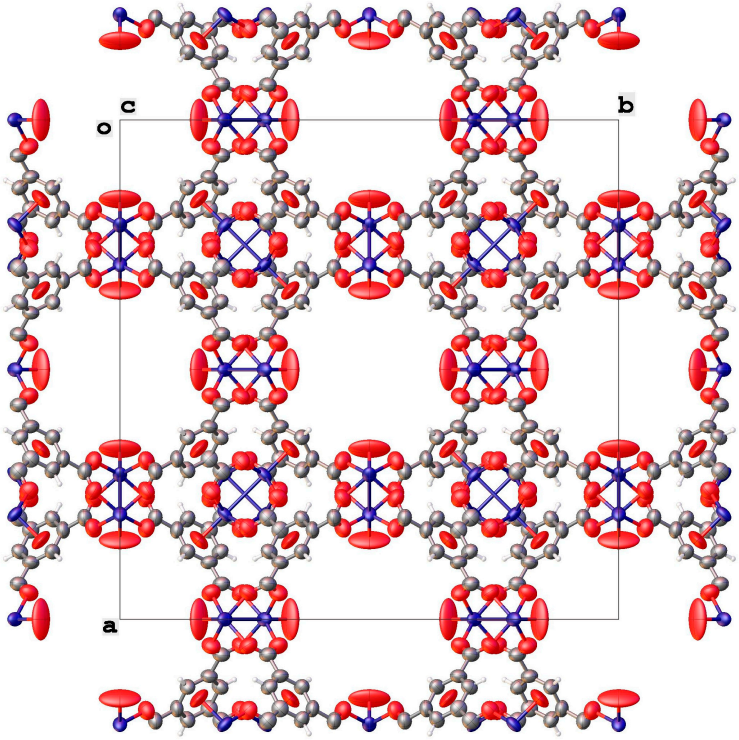


Figure 2. Packing view of the cubic Zn–BTC framework of **1** along the c crystallographic axis, illustrating the regular three-dimensional arrangement of Zn_2 paddlewheel secondary building units and highlighting the hollow columns along the 4-fold axes. Additional views of the 3D packing are provided in the Supporting Information.

3.4. Comparison of SBUs and Framework Architectures

Although both compounds originate from the same Zn–BTC chemical system, their crystal structures reveal two distinct SBUs, highlighting the strong influence of crystallization conditions on framework assembly. In the cubic structure of **1**, the formation of a binuclear Zn(II) paddlewheel SBU is associated with uniform metal coordination environments and high lattice symmetry. The presence of axial solvent coordination appears to stabilize this binuclear motif, promoting the propagation of identical SBUs throughout the framework. In contrast, the tetragonal structure of **2** features heterogeneous Zn coordination environments, resulting in a mixed-coordination SBU without direct Zn–Zn interactions. In this case, the coordination flexibility of Zn(II), combined with the participation of solvent molecules, favors the stabilization of both tetra- and hexa-coordinated metal centers within the same framework. These observations demonstrate that SBU selection in Zn–BTC frameworks is not solely dictated by ligand geometry but is highly sensitive to subtle variations in the crystallization environment. Solvent molecules play a dual role, acting both as ligands that complete metal coordination spheres and as structure-directing agents that influence SBU nuclearity and geometry.

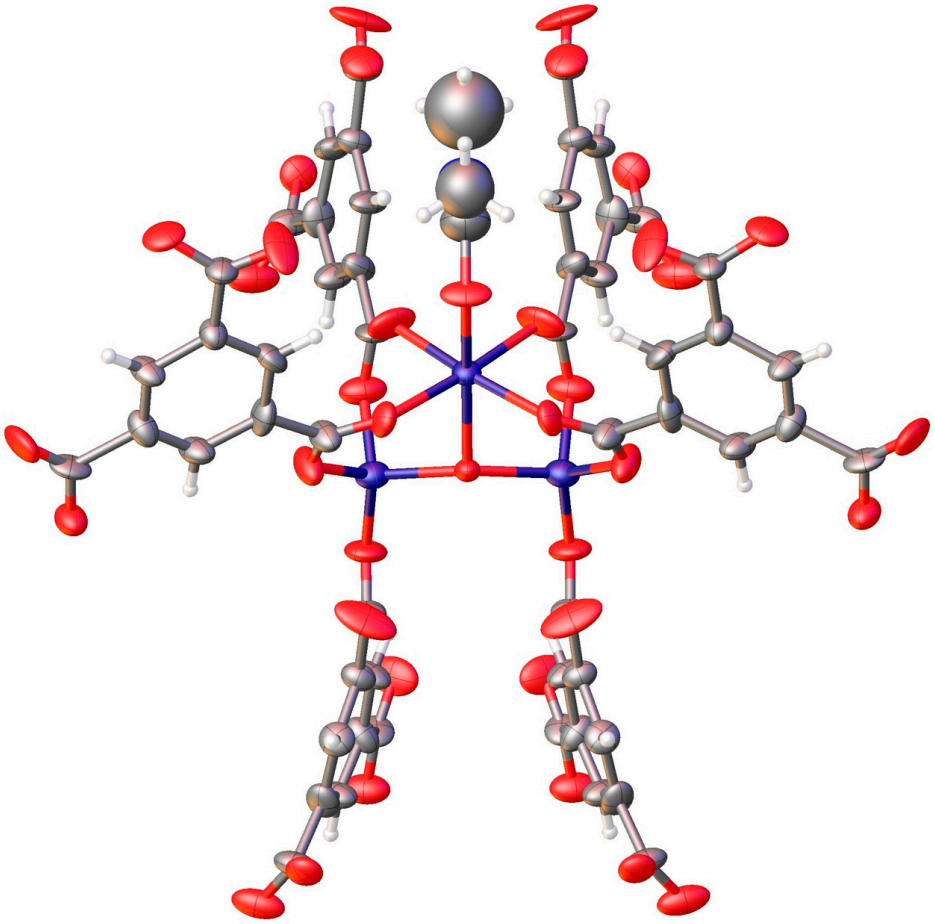


Figure 3. ORTEP representation (50% probability ellipsoids) of the Zn–based secondary building unit in the tetragonal Zn–BTC framework of **2**, showing the trinuclear unit through one crystallographic mirror plane and highlighting the coexistence of one octahedral and two equivalent tetrahedral Zn(II) coordination environments (1:2 ratio). Atom labels are omitted for clarity; full labeling is reported in the representation of the asymmetric unit in Figure S3 of Supporting Information.

3.5. Pore Structure Analysis

A geometric analysis of the pore structure was performed in order to evaluate the accessible voids in the two frameworks. The cubic framework of compound **1** exhibits a high degree of porosity, with a calculated network-accessible surface area of 1762 m^2/g and a geometric accessible volume of 0.734 cm^3/g. The pore system is characterized by a three-dimensional connectivity, as indicated by the three percolated dimensions, and by pore diameters ranging from approximately 5.36 Å (pore limiting diameter) to 11.32 Å (maximum pore diameter). These features are consistent with the high symmetry of the structure and the regular arrangement of the Zn_2 paddlewheel SBUs. In contrast, compound **2** displays a significantly lower surface area (623 m^2/g) and accessible volume (0.451 cm^3/g). The pore system is characterized by one-dimensional percolation, indicating that continuous channels are present only along a single crystallographic direction. The pore diameters range from 7.05 Å to 8.22 Å, suggesting a more constrained and less interconnected void structure. The comparison highlights how the different SBUs and coordination environments directly influence the pore architecture. The binuclear paddlewheel SBU in compound **1** promotes the formation of a highly connected three-dimensional pore network, whereas the mixed coordination SBU in compound **2** leads to reduced connectivity and more limited pore accessibility.

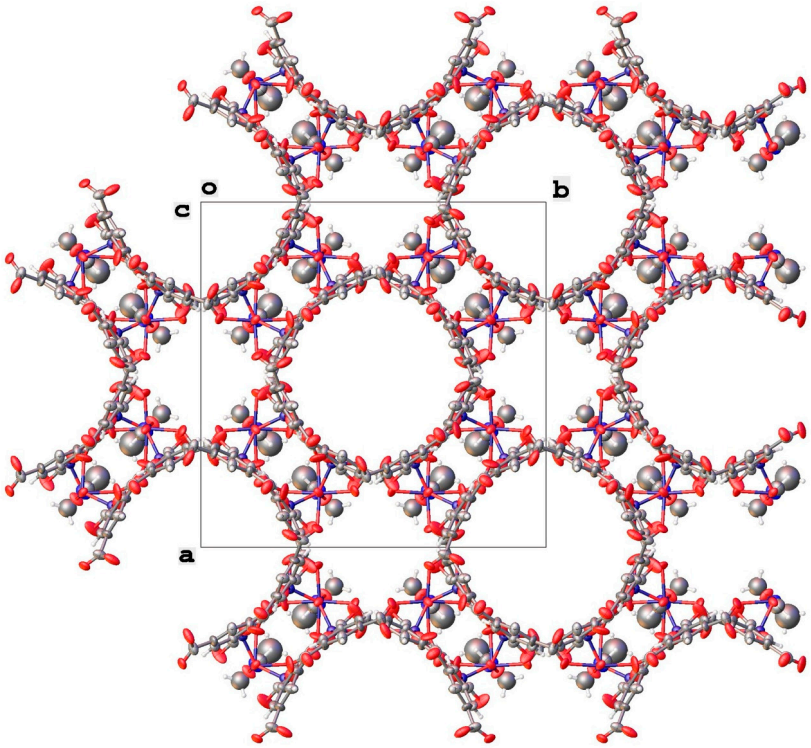


Figure 4. Packing view of the tetragonal Zn–BTC framework of **2** along the crystallographic c axis, showing the three-dimensional network formed by mixed-coordination Zn–based secondary building units and highlighting the hollow columns along the 4-fold axes. Additional views of the 3D packing are provided in the Supporting Information.

3.6. Implications for SBU Selection in Zn–BTC Systems

The comparison between these two Zn–BTC frameworks underscores the central role of Zn(II) coordination flexibility in governing SBU formation. The ability of Zn(II) to adopt multiple coordination geometries enables the emergence of alternative SBUs from identical chemical components, leading to distinct framework architectures. These results highlight the importance of detailed single-crystal structural analysis in identifying and rationalizing SBU diversity in MOF systems. Understanding how crystallization conditions influence SBU selection is essential for controlling framework topology and, ultimately, for the rational design of Zn–based MOFs with targeted structural features. From a broader perspective, the ability of Zn(II) to generate different SBUs under closely related crystallization conditions has important implications for the rational design of MOFs. Although the present study is primarily focused on structural characterization, the observed SBU variability is directly reflected in the resulting pore architecture, as demonstrated by the differences in accessible surface area, pore dimensions, and connectivity between the two frameworks. In particular, the transition from a three-dimensional pore network in compound **1** to a one-dimensional percolated system in compound **2** highlights how coordination environment and SBU topology can govern pore accessibility and dimensionality. These observations suggest that careful control of the solvent environment may represent an effective strategy to direct SBU formation and, consequently, to tune the structural and geometric properties of Zn–based frameworks.

4. Conclusions

In this work, two Zn(II)-trimesate frameworks obtained under different hydrothermal conditions were structurally characterized by single-crystal X-ray diffraction. Although both compounds originate from the same Zn–BTC chemical system, they exhibit markedly

different coordination environments and secondary building units (SBUs), highlighting the structural versatility of Zn(II) in carboxylate-based frameworks. The framework of compound **1** crystallizes in a cubic lattice and is built from a well-defined binuclear Zn_2 paddlewheel type SBU, characterized by a short Zn–Zn separation and four μ_2-bridging carboxylate groups. In contrast, the framework of compound **2** adopts a tetragonal structure and features mixed Zn(II) coordination environments, with the coexistence of tetrahedral and octahedral metal centers assembled into a fundamentally different SBU. The comparison between these two structures underscores the sensitivity of Zn–BTC frameworks to crystallization conditions, particularly solvent composition, which appears to influence Zn(II) coordination preferences and SBU selection. While no mechanistic conclusions can be drawn from the present data alone, these results emphasize the importance of detailed crystallographic analysis in revealing subtle structure–assembly relationships in metal–organic frameworks. Overall, this study contributes to the understanding of SBU diversity in Zn–trimesate systems and illustrates how identical chemical building blocks can give rise to distinct framework architectures through variations in local coordination chemistry. Such insights are relevant for the rational design of Zn–based MOFs and for future investigations aimed at controlling framework structure through targeted synthetic strategies. The pore analysis further confirms that SBU selection not only affects the structural topology but also significantly impacts the resulting pore architecture and connectivity, leading to marked differences in accessible surface area and dimensionality of the pore system. Future work will focus on systematically varying crystallization parameters in order to establish clearer correlations between solvent environment and SBU formation. In addition, further studies will be aimed at investigating the physicochemical properties of these frameworks, including their potential porosity and guest inclusion behavior.

Supplementary Materials: The following supporting information can be downloaded at: https://www.mdpi.com/article/10.3390/cryst16050290/s1. Figure S1. ORTEP view of the binuclear $Zn_2(O_2CR)_4$ moiety with the four μ_2-bridging ligands in the cubic Zn-BTC framework of **1**, showing the atomic numbering scheme of the crystallographic asymmetric unit. Ellipsoids are drawn at 50% probability level while H-atom size is arbitrary, and hydrogens of the coordinated water molecule are omitted; Figure S2. Packing representations of the cubic cell Zn-BTC framework of **1** illustrating the regular three-dimensional arrangement of Zn_2 paddlewheel secondary building units; Figure S3. View illustrating the position of the molecular unit of compound **1** relative to the selected crystallographic mirror planes; Figure S4. ORTEP view of the trinuclear moiety in the tetragonal Zn-BTC framework of **2**, showing the atomic numbering scheme of the crystallographic asymmetric unit. Ellipsoids are drawn at 50% probability level while H-atom size is arbitrary; Figure S5. Packing representations of the tetragonal Zn-BTC framework of **2** showing the three-dimensional network formed by mixed-coordination Zn-based secondary building units; Figure S6. View illustrating the position of the molecular unit of compound **2** relative to the selected crystallographic mirror planes; Table S1. Crystal data and structure refinement for **1**; Table S2. Fractional Atomic Coordinates ($\times 10^4$) and Equivalent Isotropic Displacement Parameters ($Å^2 \times 10^3$) for **1**. U_{eq} is defined as 1/3 of the trace of the orthogonalised U_{IJ} tensor; Table S3. Anisotropic Displacement Parameters ($Å^2 \times 10^3$) for **1**. The Anisotropic displacement factor exponent takes the form: $-2\pi^2[h^2a^{*2}U_{11} + 2hka^*b^*U_{12} + \ldots]$; Table S4. Bond Lengths for **1**; Table S5. Bond Angles for **1**; Table S6. Torsion Angles for **1**; Table S7. Hydrogen Atom Coordinates ($Å \times 10^4$) and Isotropic Displacement Parameters ($Å^2 \times 10^3$) for **1**; Table S8. Solvent masks information for **1**; Table S9. Crystal data and structure refinement for **2**; Table S10. Fractional Atomic Coordinates ($\times 10^4$) and Equivalent Isotropic Displacement Parameters ($Å^2 \times 10^3$) for **2**. U_{eq} is defined as 1/3 of the trace of the orthogonalised U_{IJ} tensor; Table S11. Anisotropic Displacement Parameters ($Å^2 \times 10^3$) for **2**. The Anisotropic displacement factor exponent takes the form: $-2\pi^2[h^2a^{*2}U_{11} + 2hka^*b^*U_{12} + \ldots]$; Table S12. Bond Lengths for **2**; Table S13. Bond Angles for **2**; Table S14. Torsion Angles for **2**; Table S15. Hydrogen Atom Coordinates

(Å $\times$ 10^4) and Isotropic Displacement Parameters (Å^2 $\times$ 10^3) for **2**; Table S16. Atomic Occupancy for **2**; Table S17. Solvent masks information for **2**.

Author Contributions: Conceptualization, A.S. and G.B. (Giuseppe Bruno); methodology, F.N.; software, F.N.; validation, G.B. (Giovanni Bella), A.A. and G.B. (Giuseppe Bruno); formal analysis, F.N.; investigation, A.S.; resources, G.B. (Giuseppe Bruno); data curation, G.B. (Giovanni Bella); writing—original draft preparation, A.S.; writing—review and editing, G.B. (Giovanni Bella), G.B. (Giuseppe Bruno) and F.N.; visualization, A.A.; supervision, F.N.; project administration, A.S. All authors have read and agreed to the published version of the manuscript.

Funding: This research received no external funding.

Data Availability Statement: Crystallographic data are exhaustively reported in Supporting Information, and the .cif files are available on the CCDC by using the code 2539925 for **1** and 2539926 for **2**.

Conflicts of Interest: The authors declare no conflicts of interest.

References

1. Kunnummal, A.; Parambil, R.A.; Maniappan, S.; Kumar, J. Upconverted Chiral Emission in Hybrid Photonic Nanomaterials: Toward Amplified Circularly Polarized Luminescence with Tunable Chirality. *ACS Appl. Opt. Mater.* **2024**, *2*, 2451–2458. [CrossRef]
2. Keerthana, L.; Zhang, Y.; Yang, B.; Ji, J.; Bi, J.; Gong, H. Review of Photon Upconversion Nanomaterials for High-Throughput Applications. *ACS Appl. Nano Mater.* **2026**, *9*, 5246–5267. [CrossRef]
3. Lu, W.; Zhang, J.; Li, Y.S.; Chen, Q.; Wang, X.; Hassanien, A.; Chen, L. Contactless Characterization of Electronic Properties of Nanomaterials Using Dielectric Force Microscopy. *J. Phys. Chem. C* **2012**, *116*, 7158–7163. [CrossRef]
4. Wu, D.; Kusada, K.; Nanba, Y.; Koyama, M.; Yamamoto, T.; Toriyama, T.; Matsumura, S.; Seo, O.; Gueye, I.; Kim, J.; et al. Noble-Metal High-Entropy-Alloy Nanoparticles: Atomic-Level Insight into the Electronic Structure. *J. Am. Chem. Soc.* **2022**, *144*, 3365–3369. [CrossRef]
5. Ma, Z.; Mohapatra, J.; Wei, K.; Liu, J.P.; Sun, S. Magnetic Nanoparticles: Synthesis, Anisotropy, and Applications. *Chem. Rev.* **2023**, *123*, 3904–3943. [CrossRef]
6. Razzhivina, M.E.; Rukhlenko, I.D.; Tepliakov, N.V. Chiral Optical Properties of Möbius Graphene Nanostrips. *J. Phys. Chem. Lett.* **2023**, *14*, 4426–4432. [CrossRef] [PubMed]
7. Kumar, V.; Páez, J.L.; Míguez-Lago, S.; Cuerva, J.M.; Cruz, C.M.; Campaña, A.G. Chiral nanographenes exhibiting circularly polarized luminescence. *Chem. Soc. Rev.* **2025**, *54*, 4922–4947. [CrossRef] [PubMed]
8. Bella, G.; Bruno, G.; Santoro, A. Ball Pivoting Algorithm and discrete gaussian curvature: A direct way to curved nanographene circularly polarized luminescence spectral simulation. *FlatChem* **2023**, *42*, 100567. [CrossRef]
9. Bella, G.; Bruno, G.; Santoro, A. Circular dichroism simulations of chiral buckybowls by means curvature analyses. *FlatChem* **2023**, *40*, 100509. [CrossRef]
10. Bella, G.; Milone, M.; Bruno, G.; Santoro, A. Triphasic circularly polarized luminescence switch quantum simulation of a topologically chiral catenane. *J. Mater. Chem. C* **2024**, *12*, 3005–3012. [CrossRef]
11. Yaghi, O.M.; O'Keeffe, M.; Ockwig, N.W.; Chae, H.K.; Eddaoudi, M.; Kim, J. Reticular synthesis and the design of new materials. *Nature* **2003**, *423*, 705–714. [CrossRef]
12. Furukawa, H.; Cordova, K.E.; O'Keeffe, M.; Yaghi, O.M. The Chemistry and Applications of Metal-Organic Frameworks. *Science* **2013**, *341*, 1230444. [CrossRef]
13. Kitagawa, S.; Kitaura, R.; Noro, S.-i. Functional Porous Coordination Polymers. *Angew. Chem. Int. Ed.* **2004**, *43*, 2334–2375. [CrossRef]
14. Zhou, H.-C.J.; Kitagawa, S. Metal–Organic Frameworks (MOFs). *Chem. Soc. Rev.* **2014**, *43*, 5415–5418. [CrossRef] [PubMed]
15. Li, J.-R.; Kuppler, R.J.; Zhou, H.-C. Selective gas adsorption and separation in metal–organic frameworks. *Chem. Soc. Rev.* **2009**, *38*, 1477–1504. [CrossRef]
16. Stock, N.; Biswas, S. Synthesis of Metal-Organic Frameworks (MOFs): Routes to Various MOF Topologies, Morphologies, and Composites. *Chem. Rev.* **2012**, *112*, 933–969. [CrossRef]
17. Férey, G. Hybrid porous solids: Past, present, future. *Chem. Soc. Rev.* **2008**, *37*, 191–214. [CrossRef] [PubMed]
18. Ibrahim, Y.; Mahmood, F.; Sinopoli, A.; Moursi, A.; Mahmoud, K.A.; Al-Ansari, T. Advancements of metal-organic frameworks for atmospheric water harvesting and climate control. *J. Water Process Eng.* **2024**, *67*, 106249. [CrossRef]

19. Chui, S.S.-Y.; Lo, S.M.-F.; Charmant, J.P.H.; Orpen, A.G.; Williams, I.D. A Chemically Functionalizable Nanoporous Material. *Science* **1999**, *283*, 1148–1150. [CrossRef]
20. Li, H.; Eddaoudi, M.; O'Keeffe, M.; Yaghi, O.M. Design and synthesis of an exceptionally stable and highly porous metal-organic framework. *Nature* **1999**, *402*, 276–279. [CrossRef]
21. Rowsell, J.L.C.; Yaghi, O.M. Metal–organic frameworks: A new class of porous materials. *Microporous Mesoporous Mater.* **2004**, *73*, 3–14. [CrossRef]
22. Pettinari, C.; Tăbăcaru, A.; Galli, S. Coordination polymers and metal–organic frameworks based on poly(pyrazole)-containing ligands. *Coord. Chem. Rev.* **2016**, *307*, 1–31. [CrossRef]
23. Robin, A.Y.; Fromm, K.M. Coordination polymer networks with O- and N-donors: What they are, why and how they are made. *Coord. Chem. Rev.* **2006**, *250*, 2127–2157. [CrossRef]
24. Santoro, A.; Holub, J.; Fik-Jaskółka, M.A.; Vantomme, G.; Lehn, J.-M. Dynamic Helicates Self-Assembly from Homo- and Heterotopic Dynamic Covalent Ligand Strands. *Chem.-A Eur. J.* **2020**, *26*, 15664–15671. [CrossRef] [PubMed]
25. Holub, J.; Santoro, A.; Lehn, J.-M. Electronic absorption and emission properties of bishydrazone [2 × 2] metallosupramolecular grid-type architectures. *Inorganica Chim. Acta* **2019**, *494*, 223–231. [CrossRef]
26. Eddaoudi, M.; Kim, J.; Rosi, N.; Vodak, D.; Wachter, J.; O'Keeffe, M.; Yaghi, O.M. Systematic Design of Pore Size and Functionality in Isoreticular MOFs and Their Application in Methane Storage. *Science* **2002**, *295*, 469–472. [CrossRef]
27. Zhou, H.-C.; Long, J.R.; Yaghi, O.M. Introduction to Metal–Organic Frameworks. *Chem. Rev.* **2012**, *112*, 673–674. [CrossRef]
28. Eddaoudi, M.; Moler, D.B.; Li, H.; Chen, B.; Reineke, T.M.; O'Keeffe, M.; Yaghi, O.M. Modular Chemistry: Secondary Building Units as a Basis for the Design of Highly Porous and Robust Metal–Organic Carboxylate Frameworks. *Acc. Chem. Res.* **2001**, *34*, 319–330. [CrossRef]
29. O'Keeffe, M.; Yaghi, O.M. Deconstructing the Crystal Structures of Metal–Organic Frameworks and Related Materials into Their Underlying Nets. *Chem. Rev.* **2012**, *112*, 675–702. [CrossRef] [PubMed]
30. Rowsell, J.L.C.; Yaghi, O.M. Strategies for Hydrogen Storage in Metal–Organic Frameworks. *Angew. Chem. Int. Ed.* **2005**, *44*, 4670–4679. [CrossRef]
31. Batten, S.R.; Robson, R. Interpenetrating Nets: Ordered, Periodic Entanglement. *Angew. Chem. Int. Ed.* **1998**, *37*, 1460–1494. [CrossRef]
32. Moulton, B.; Zaworotko, M.J. From Molecules to Crystal Engineering: Supramolecular Isomerism and Polymorphism in Network Solids. *Chem. Rev.* **2001**, *101*, 1629–1658. [CrossRef]
33. Friščić, T.; MacGillivray, L.R. Engineering cocrystal and polymorph architecture via pseudoseeding. *Chem. Commun.* **2009**, *7*, 773–775. [CrossRef]
34. Qin, L.; Li, Y.; Ma, D.; Liang, F.; Chen, L.; Xie, C.; Lin, J.; Pan, Y.; Li, G.; Chen, F.; et al. Two transition metal-organic frameworks based on 5-phenyl-isophthalate and N-donor mixed ligands: Structure, magnetic, drug delivery and catalytic properties. *J. Solid State Chem.* **2022**, *312*, 123175. [CrossRef]
35. Liang, F.; Ma, D. Luminescence and catalytic properties of two nickel(II)-organic frameworks constructed by 5-substituted isophthalate and N-donor mixed ligands. *J. Mol. Struct.* **2020**, *1208*, 127814. [CrossRef]
36. Yan, P.; Chen, Z.; Li, X.; Liang, F.; Tan, Y.; Lin, Y.; Yang, K.; Xiao, C.; Wu, J.; Ma, D. Tuning the CO_2 selective adsorption performance in MOFs by incorporating functional groups on the isophthalate skeleton. *J. Solid State Chem.* **2024**, *330*, 124461. [CrossRef]
37. Zhao, H.; Li, L.; Li, J.; Yan, F.; Wang, W.; Zhao, M. A Novel Zn-Cu Bimetallic Mixed-Component MOFs Composite for Efficient CO_2 Capture. *Nanomaterials* **2025**, *15*, 1777. [CrossRef]
38. Manos, M.J.; Moushi, E.E.; Papaefstathiou, G.S.; Tasiopoulos, A.J. New Zn^{2+} Metal Organic Frameworks with Unique Network Topologies from the Combination of Trimesic Acid and Amino-Alcohols. *Cryst. Growth Des.* **2012**, *12*, 5471–5480. [CrossRef]
39. Huang, X.-C.; Lin, Y.-Y.; Zhang, J.-P.; Chen, X.-M. Ligand-Directed Strategy for Zeolite-Type Metal–Organic Frameworks: Zinc(II) Imidazolates with Unusual Zeolitic Topologies. *Angew. Chem. Int. Ed.* **2006**, *45*, 1557–1559. [CrossRef]
40. Ma, S.; Zhou, H.-C. Gas storage in porous metal–organic frameworks for clean energy applications. *Chem. Commun.* **2010**, *46*, 44–53. [CrossRef]
41. Suh, M.P.; Park, H.J.; Prasad, T.K.; Lim, D.-W. Hydrogen Storage in Metal–Organic Frameworks. *Chem. Rev.* **2012**, *112*, 782–835. [CrossRef]
42. Moloto, W.; Mbule, P.; Nxumalo, E.; Ntsendwana, B. Stabilizing effects of zinc(II)-benzene-1,3,5-tricarboxylate metal organic frameworks on the performance of TiO_2 photoanodes for use in dye-sensitized solar cells. *J. Photochem. Photobiol. A Chem.* **2021**, *407*, 113063. [CrossRef]
43. Scatena, R.; Guntern, Y.T.; Macchi, P. Electron Density and Dielectric Properties of Highly Porous MOFs: Binding and Mobility of Guest Molecules in $Cu_3(BTC)_2$ and $Zn_3(BTC)_2$. *J. Am. Chem. Soc.* **2019**, *141*, 9382–9390. [CrossRef]
44. Degaga, G.D.; Pandey, R.; Gupta, C.; Bharadwaj, L. Tailoring of the electronic property of Zn-BTC metal–organic framework via ligand functionalization: An ab initio investigation. *RSC Adv.* **2019**, *9*, 14260–14267. [CrossRef]

45. Lalawmpuia, R.; Lalhruaitluangi, M.; Lalhmunsiama; Tiwari, D. Metal organic framework (MOF): Synthesis and fabrication for the application of electrochemical sensing. *Environ. Eng. Res.* **2024**, *29*, 230636. [CrossRef]
46. Friščić, T.; Jones, W. Recent Advances in Understanding the Mechanism of Cocrystal Formation via Grinding. *Cryst. Growth Des.* **2009**, *9*, 1621–1637. [CrossRef]
47. Timofeeva, M.V.; Yankin, A.N. Synthesis and characterization of ZnBTC-based MOFs: Effect of solvents and salt. *Chim. Techno Acta* **2022**, *10*, 202310105. [CrossRef]
48. Spek, A. Structure validation in chemical crystallography. *Acta Crystallogr. Sect. D* **2009**, *65*, 148–155. [CrossRef]
49. Spek, A. PLATON SQUEEZE: A tool for the calculation of the disordered solvent contribution to the calculated structure factors. *Acta Crystallogr. Sect. C* **2015**, *71*, 9–18. [CrossRef]
50. Sylvain, R.; Vendier, L.; Bijani, C.; Santoro, A.; Puntoriero, F.; Campagna, S.; Sutra, P.; Igau, A. Evidence of the unprecedented conversion of intermolecular proton to water bridging of two phosphoryl ruthenium complexes. *New J. Chem.* **2013**, *37*, 3543–3548. [CrossRef]
51. Sheldrick, G. SHELXT—Integrated space-group and crystal-structure determination. *Acta Crystallogr. Sect. A* **2015**, *71*, 3–8. [CrossRef]
52. Sheldrick, G. Crystal structure refinement with SHELXL. *Acta Crystallogr. Sect. C* **2015**, *71*, 3–8. [CrossRef] [PubMed]
53. Blatov, V.A.; Shevchenko, A.P.; Proserpio, D.M. Applied Topological Analysis of Crystal Structures with the Program Package ToposPro. *Cryst. Growth Des.* **2014**, *14*, 3576–3586. [CrossRef]
54. Bruker, A. *SAINT-Plus and SADABS*; Bruker AXS Inc.: Madison, WI, USA, 2004.
55. Bruker, A. *APEX2, SADABS and SAINT*; Bruker AXS Inc.: Madison, WI, USA, 2010.
56. Dolomanov, O.V.; Bourhis, L.J.; Gildea, R.J.; Howard, J.A.K.; Puschmann, H. OLEX2: A complete structure solution, refinement and analysis program. *J. Appl. Crystallogr.* **2009**, *42*, 339–341. [CrossRef]

Disclaimer/Publisher's Note: The statements, opinions and data contained in all publications are solely those of the individual author(s) and contributor(s) and not of MDPI and/or the editor(s). MDPI and/or the editor(s) disclaim responsibility for any injury to people or property resulting from any ideas, methods, instructions or products referred to in the content.